Tensor analyzing powers and energy dependence of the ^{7}Li+^{16}O interaction

A. T. Rudchik,[1,*] K. W. Kemper,[2] A. A. Rudchik,[1] A. M. Crisp,[2] V. D. Chesnokova,[1] V. M. Kyryanchuk,[1] F. Maréchal,[2] O. A. Momotyuk,[1,2] O. A. Ponkratenko,[1] B. T. Roeder,[2] and K. Rusek[3]

[1]*Institute for Nuclear Research, Prospect Nauki 47, 03680 Kyiv, Ukraine*

[2]*Physics Department, Florida State University, Tallahassee, Florida 32306-4350, USA*

[3]*Institute for Nuclear Studies, A. Soltan Hoża 69, PL-00-681 Warsaw, Poland*

(Received 20 July 2006; published 28 February 2007)

The differential cross section angular distribution and the analyzing powers $^{T}T_{10}$, $^{T}T_{20}$, for ^{7}Li+^{16}O elastic scattering were measured at $E_{\rm lab}(^{7}\vec{\rm Li}) = 42$ MeV. These and previously published ^{7}Li+^{16}O scattering data measured at $E_{\rm c.m.} = 6.26-34.78$ MeV were analyzed with the optical model and coupled-reaction channels (CRC) methods to determine the energy dependence of the parameters of the scattering potential. It was found that the optical model potentials are energy independent for ^{7}Li laboratory bombarding energies above 28 MeV, except for a slight decrease in the real potential strength as the bombarding energy increases. The calculations presented show that the tensor analyzing power $^{T}T_{20}$ arises from a coherent combination of contributions from the ground-state reorientation and central scattering potential. The energy-dependent CRC potentials were shown to describe the data for the ^{16}O(^{7}Li,t)^{20}Ne reaction.

DOI: 10.1103/PhysRevC.75.024612 PACS number(s): 25.70.Bc, 24.10.Eq, 25.70.Hi, 24.70.+s

I. INTRODUCTION

As the ability to carry out scattering and reaction studies with exotic beams increases, it is important to have knowledge of elastic-scattering potentials for stable nuclei because they aid in the identification of new mechanisms that contribute to the scattering. However, the elastic-scattering data needed to determine these potentials at the energy of the reaction studies are often not available for exotic nuclei, and often the reaction studies are carried out at different energies from those of the elastic scattering. Therefore, knowledge of the energy dependence of the elastic-scattering potentials is necessary to develop calculations to study the mechanisms contributing to the scattering. This knowledge is particularly important at energies in the nuclear scattering regime because the contribution of many different channels affects the observed elastic-scattering cross section.

The present work reports a study of the energy dependence of the elastic-scattering potential of ^{7}Li+^{16}O. This system was chosen because the excitation of states in ^{16}O is weak, reducing the influence of its excited states on the underlying central potential. Due to this, the ^{7}Li+^{16}O system is well suited for a study of the energy dependence of the projectile on the elastic-scattering potential. An understanding of ^{7}Li scattering can serve also as a surrogate for other light exotic nuclei with large ground-state quadrupole moments such as ^{7}Be, ^{8}Li, and ^{8}B. The influence of the ground-state quadrupole moment of ^{7}Li on the scattering is clearly observed by measuring its tensor analyzing powers, which arise from the ground-state reorientation of ^{7}Li as it scatters [1]. Thus, a reproduction of the tensor analyzing powers for ^{7}Li elastic scattering means that the influence of the ground-state quadrupole moment on the elastic scattering is properly included in the calculation. Because ^{7}Li, while stable, is similar to other light exotic nuclei, the development of global elastic-scattering potential parameters for ^{7}Li scattering will serve as a good starting point in the development of future calculations for elastic scattering and reaction studies for exotic light nuclei.

To study the energy dependence of the potential parameters for the ^{7}Li+^{16}O system, previously reported data [2–7] were analyzed along with new data reported here at 42 MeV with the optical model (OM) and coupled-reaction channels method (CRC) [8] to determine the energy dependence of the central scattering potential. Recent studies of ^{7}Li+^{11}B [9], ^{14}N [10] showed that the reorientation of ^{7}Li produced the larger than expected cross sections at large angles and so this work concentrates on the forward angle scattering.

To determine the potentials, the data were fitted at each energy by the OM and CRC methods independently, and then the parameters were corrected step by step using the procedure outlined in Ref. [11] to obtain the energy dependence of the scattering potentials. In this way, it was found that the scattering potentials are almost energy independent for ^{7}Li bombarding energies above about 28 MeV.

To illustrate the usefulness of the developed scattering potential, an analysis of the ^{16}O(^{7}Li,t)^{20}Ne reaction data at different energies is included to demonstrate the reliability of the deduced energy dependence of the ^{7}Li+^{16}O potential parameters.

The article is organized as follows. Section II describes the new experimental results, Sec. III presents the OM and CRC calculations, and Sec. IV gives the conclusions.

II. EXPERIMENTAL PROCEDURE

A polarized $^{7}\vec{\rm Li}$ beam was produced by the Florida State University (FSU) optically pumped polarized Li ion source (OPPLIS) [12]. The beam was then accelerated by the FSU Tandem/Linac accelerator to $E_{\rm lab} = 42$ MeV and bombarded a 150-μg/cm^2 ^{6}Li target. The ^{6}Li target was prepared with

*Electronic address: rudchik@kinr.kiev.ua

vacuum evaporation of lithium on a thin formvar foil and was transferred under static vacuum to the scattering chamber to minimize oxidation. The small amount of oxidation that occurred during the transfer of the targets to the scattering chamber was sufficient to extract the angular distribution and analyzing power data.

Two silicon surface barrier ΔE-E counter telescopes were used for detecting the reaction products. These detectors were placed to the left and right of the beam at equal angles. The E detectors were 1000 μm (left) and 1500 μm (right) thick and the ΔE detectors were both 75 μm. The beam polarization on target was monitored by the reaction ^{4}He($\vec{^7}$Li,^{7}Li) [13]. The beam polarizations were $t_{10} = 0.76 \pm 0.07$, $t_{20} = 0.37 \pm 0.07$, and $t_{30} = 0.14 \pm 0.07$. The equations for calculations of polarization and analyzing powers measured on target were taken from Ref. [14].

Even though the scattering chamber has a reasonable vacuum it is still possible that the amount of oxygen on the Li target could change during the experiment, thus changing the experimental results. Consequently, a monitor detector was used for the angular distribution and by dividing by the number of counts in it during a given run, a relative angular distribution was obtained at 42 MeV. The absolute cross section was obtained by normalizing the forward-angle 42-MeV data to that published earlier at 34 MeV in short runs. The possible buildup of oxygen on the target during the analyzing power measurements did not affect these results because checks of the oxygen yield during the polarization off state showed no measurable buildup in oxygen during one cycle of the analyzing power measurement, which takes about 8 min to cycle through all the beam polarization states.

The measured angular distribution and analyzing powers of $^T T_{10}$, $^T T_{20}$ for the ^{7}Li+^{16}O elastic scattering at the energy $E_{\rm lab}(\vec{^7}{\rm Li}) = 42$ MeV are shown in Figs. 1 and 2.

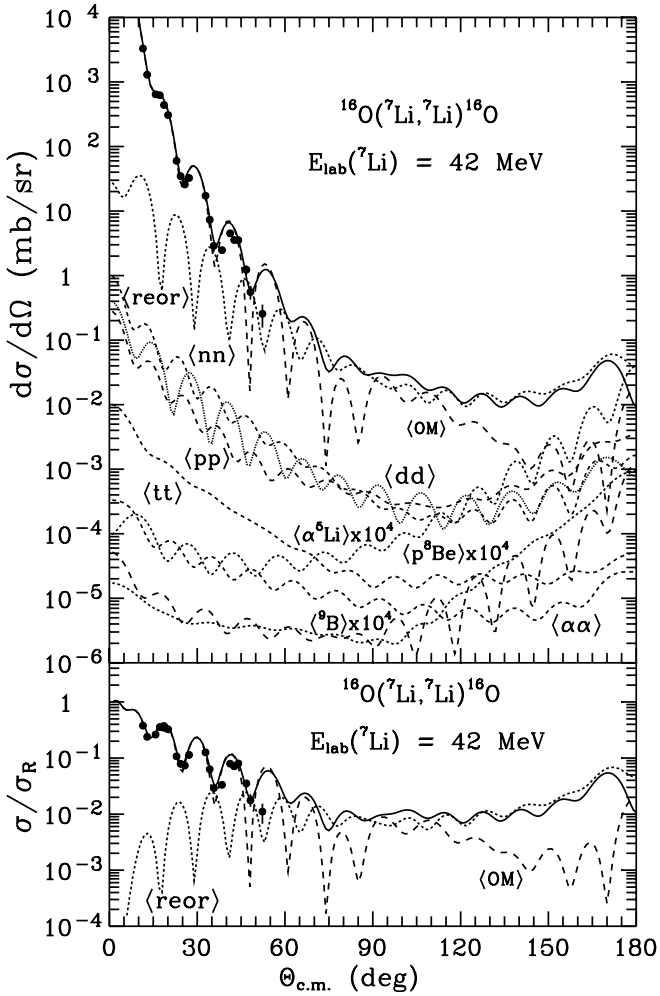

FIG. 1. Angular distribution of the ^{7}Li+^{16}O elastic scattering at $E_{\rm lab}(^7{\rm Li}) = 42$ MeV. The curves show the OM cross section (curves ⟨OM⟩) and CRC calculations for the reorientation of ^{7}Li (curves ⟨reor⟩), ^{9}B-cluster transfer (curve ⟨^{9}B⟩), sequential transfers of neutrons (curve ⟨nn⟩), protons (curve ⟨pp⟩), clusters d+d (curve ⟨dd⟩), t+t (curve ⟨tt⟩), α+α (curve ⟨$\alpha\alpha$⟩), p+^{8}Be (curve ⟨p^{8}Be⟩), and α + ^{5}Li (curve ⟨α^5Li⟩). The solid curves show the coherent sum of all processes.

III. ANALYSIS OF THE DATA

A. Calculation procedure

The calculation procedure used in the present work was similar to that of Ref. [9]. A Woods-Saxon potential of the form $U(r) = V(r) + iW_S(r)$ with the parameters $X = \{X_i\} = \{V_0, r_V, a_V, W_S, r_W, a_W\}$ and the Coulomb potential of a uniform charged sphere were used in the OM and CRC calculations. The potential radii were calculated as $R_i = r_i(A_P^{1/3}+A_T^{1/3})$ $(i = V, W, C)$. The Coulomb potential parameter r_C was fixed at the value of 1.25 fm.

The potential parameters were fitted to the data at each energy as follows. First, the data were fitted within the OM using only the elastic-scattering data (OM fitting) with the code SPI-GENOA [15]. The potential developed in the OM was then used as the initial potential in CRC calculations using the code FRESCO [8] to describe the data of all nuclear processes included in the analysis (CRC fitting). In the CRC calculations, it was mainly the parameters of the imaginary potential that were adjusted (in particular, parameter W_S). For some data, it was also necessary to slightly vary the parameters of the real potential. The conventional optical model parameters found in this study are given in Table I and the resulting OM and CRC calculations with these parameters are shown in the figures.

The elastic and inelastic transitions shown in Fig. 3 and the transfers represented by the diagrams in Fig. 4 were included in the CRC coupling scheme. The results of these calculations and the channels important in the scattering are discussed in the following sections.

The present calculations contain data only for forward angles, where it might be expected that contributions to the scattering arising from particle transfer reactions would be weak. For completeness, these effects were included and are shown in the plots of the data. In the CRC calculations, the necessary spectroscopic amplitudes S_x of transferred clusters or nucleons x in the systems $A = C + x$ were calculated within the translational-invariant shell model (TISM) [16] using the code DESNA [17,18] and Boyarkina's wave function

TABLE I. Parameters of the ^{7}Li+^{16}O and $t + ^{20}$Ne potentials. The A_i parameters are the results of both OM and CRC fits, whereas the C_i parameters are from the CRC calculations. The B_i parameters are taken from the indicated references.

E_{lab} (MeV)	$E_{c.m.}$ (MeV)	Sets	V (MeV)	r_V (fm)	a_V (fm)	W_S (MeV)	r_W (fm)	a_W (fm)	r_C (fm)	c_V	c_W
					^{7}Li+^{16}O						
9 [5]	6.26	A_1	59.0	0.980	0.651	4.5	1.250	0.651	1.25	10.75	10.02
13 [5]	9.04	A_2	86.2	0.980	0.673	6.0	1.220	0.673	1.25	10.91	9.83
15 [21]	10.43	C_1	87.3	0.903	0.658	5.3	1.331	0.658	1.25	10.55	10.63
36 (^{16}O) [3]	10.96	A_3	95.6	0.802	0.648	4.5	1.250	0.648	1.25	10.05	10.06
		B_3 [3]	10.5	0.848	0.658	3.4	0.848	0.658	0.56	8.06	6.94
20 [2]	13.91	A_4	154.3	0.970	0.690	11.3	1.283	0.690	1.25	11.27	10.67
		B_4 [2]	33.1	0.980	0.850	10.3[b]	1.063	0.720	1.42	8.61	7.88
30.3 [22]	21.07	C_2	195.9	0.805	0.696	14.8	1.204	0.696	1.25	10.40	10.36
34 [7]	23.17[a]	A_5	181.0	0.860	0.730	15.4	1.300	0.730	1.25	10.42	10.63
		A_{15}	181.0	0.802	1.000	15.4	1.300	1.000	1.25	8.75	8.50
34 [7]	23.65	A_6	180.7	0.802	0.700	15.4	1.206	0.700	1.25	10.28	10.37
		B_6 [7]	240.6	0.676	0.730	16.3	1.182	0.710	0.74	9.59	10.17
34 [23]	23.65	C_3	188.8	0.803	0.698	15.5	1.201	0.698	1.25	10.34	10.37
36 [4]	25.04	A_7	179.6	0.807	0.700	15.6	1.203	0.700	1.25	10.30	10.37
		B_7 [4]	189.5	0.688	0.743	21.3	1.137	0.821	0.74	9.35	9.20
38 [24]	26.43	C_4	182.9	0.802	0.699	15.8	1.200	0.699	1.25	10.30	10.37
42	29.22	A_8	175.1	0.802	0.700	16.0	1.200	0.700	1.25	10.24	10.37
50 [6]	34.78	A_9	170.8	0.802	0.700	16.5	1.200	0.700	1.25	10.22	10.38
		B_9 [6]	170.3	0.688	0.777	11.4	1.194	0.951	0.74	9.06	8.00
9, 20, 36		B_{10} [5]	195.0	0.680	0.740	55.0[b]	0.680	0.740	0.68	9.35	8.08
					t+^{20}Ne						
	12.70 [21]	D_1	142.0	0.855	0.829	16.0	1.800	0.829	1.25	9.24	11.80
	23.34 [22]	D_2	142.0	0.855	0.829	16.0	1.600	0.829	1.25	9.24	10.80
	25.92 [23]	D_3	142.0	0.855	0.829	16.0	1.700	0.829	1.25	9.24	11.30
	28.70 [24]	D_3	142.0	0.855	0.829	16.0	1.800	0.829	1.25	9.24	11.80

[a]The potential parameters for the 0.478-MeV excited state of ^{7}Li.
[b]The surface imaginary potential.

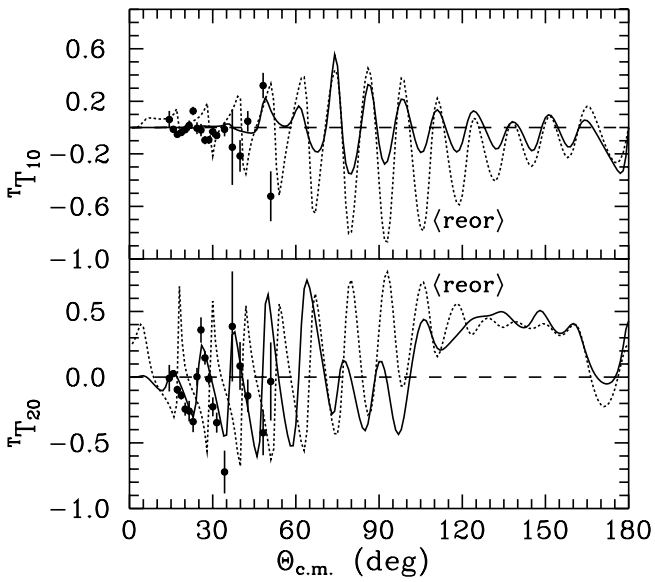

FIG. 2. Analyzing powers of $^T T_{10}$, $^T T_{20}$ for the ^{7}Li+^{16}O elastic scattering at $E_{lab}(^7\text{Li}) = 42$ MeV. The curves show the CRC calculations for the reorientation of ^{7}Li (curves ⟨reor⟩) and coherent sum of this process together with the potential scattering (solid curves).

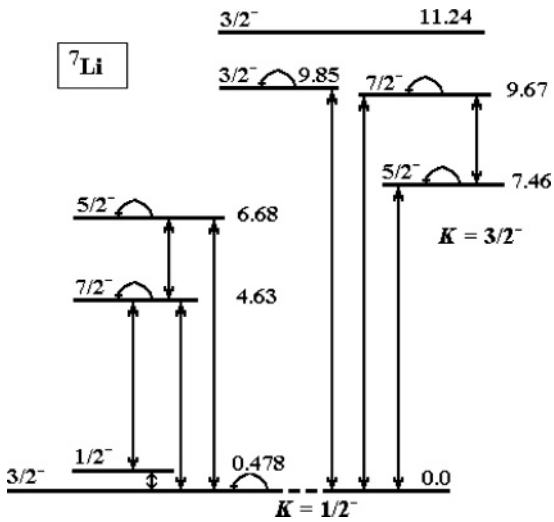

FIG. 3. Coupling schemes for the transitions to the excited state of ^{7}Li.

TABLE II. Spectroscopic amplitudes S_x of the x clusters in the $A = C + x$ systems.

A	C	x	nL_j	S_x
^{4}He	^{3}H	p	$1S_{1/2}$	1.414[a]
^{5}He	^{3}H	d	$1P_1$	0.456
			$1P_2$	1.021[a]
^{6}He	^{3}H	t	$2S_{1/2}$	−1.333[a]
^{6}Li	^{3}H	^{3}He	$2S_{1/2}$	0.943
^{7}Li	^{3}H	α	$2P_1$	1.091
^{7}Li	^{4}He	t	$2P_{3/2}$	−1.091
^{7}Li	^{5}He	d	$2S_1$	−0.674[a]
			$1D_1$	−1.205[a]
			$1D_3$	0.676[a]
^{7}Li	^{6}He	p	$1P_{3/2}$	0.805
^{7}Li$^{*}_{0.478}$	^{6}He	p	$1P_{1/2}$	0.805
^{7}Li	^{6}Li	n	$1P_{1/2}$	−0.657
			$1P_{3/2}$	−0.735[a]
^{7}Li$^{*}_{0.478}$	^{6}Li	n	$1P_{1/2}$	0.329[a]
			$1P_{3/2}$	0.930
^{8}Li	^{7}Li	n	$1P_{1/2}$	0.478
^{8}Li	^{7}Li$^{*}_{0.478}$	n	$1P_{3/2}$	0.478
^{8}Be	^{7}Li	p	$1P_{3/2}$	1.234[a]
^{8}Be	^{7}Li$^{*}_{0.478}$	p	$1P_{1/2}$	0.873[a]
^{9}Be	^{7}Li	d	$2S_1$	−0.226[a]
			$1D_1$	0.111[a]
			$1D_3$	−0.624[a]
^{10}Be	^{7}Li	t	$2P_{3/2}$	0.392[a]
^{11}B	^{7}Li	α	$3S_0$	−0.638
			$2D_2$	−0.422
^{12}C	^{7}Li	^{5}Li	$3S_{3/2}$	−0.793[a]
			$2D_{3/2}$	−0.525[a]
^{15}N	^{7}Li	^{8}Be	$2D_2$	0.226[a]
^{16}O	^{7}Li	^{9}B	$3S_{3/2}$	−0.533[a]
			$1D_{3/2}$	−0.353[a]
^{16}O	^{8}Be	^{8}Be	$3S_0$	0.365
^{16}O	^{11}B	^{5}Li	$3S_{3/2}$	−0.677[a]
			$2D_{3/2}$	−0.448[a]
^{16}O	^{12}C	α	$3S_0$	0.544
^{16}O	^{13}N	t	$2P_{1/2}$	−0.910[a]
^{16}O	^{14}N	d	$1D_1$	1.400
^{16}O	^{15}N	p	$1P_{1/2}$	−1.461[a]
^{16}O	^{15}O	n	$1P_{1/2}$	1.461[a]
^{17}O	^{16}O	n	$1D_{5/2}$	0.500
^{17}F	^{16}O	p	$1D_{5/2}$	−0.500
^{18}F	^{16}O	d	$3S_1$	1.061
^{19}F	^{16}O	t	$4S_{1/2}$	−1.091
^{20}Ne	^{16}O	α	$5S_0$	1.225
^{20}Ne	^{17}O	^{3}He	$3D_{5/2}$	−1.102[a]
^{20}Ne	^{17}F	t	$3D_{5/2}$	−1.102[a]
^{20}Ne	^{18}F	d	$3S_1$	1.217
^{20}Ne	^{19}F	p	$2S_{1/2}$	1.234[a]

[a] $S_{\text{FRESCO}} = (-1)^{J_C+j-J_A} S_x = -S_x$.

tables [19]. The amplitudes S_x calculated with DESNA are listed in Table II.

The bound cluster wave function was calculated by fitting the Woods-Saxon potential parameter V to the x-cluster binding energy for $a = 0.65$ fm and $r_V = 1.25A^{1/3}/(C^{1/3} + x^{1/3})$ fm.

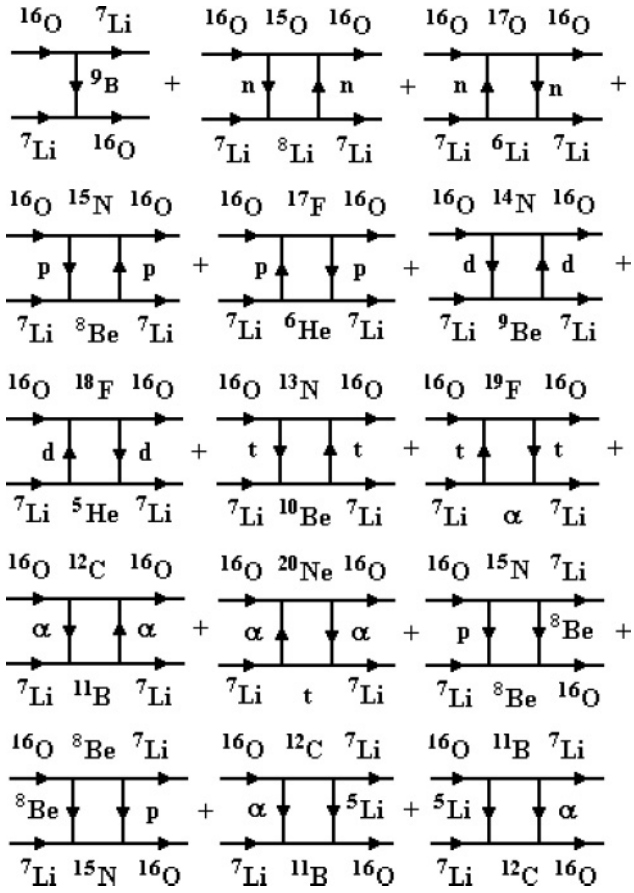

FIG. 4. Diagrams of one- and two-step transfers contributing to the ^{7}Li+^{16}O elastic-scattering calculations.

B. Determination of the elastic-scattering parameters

The angular distribution data of the ^{7}Li+^{16}O elastic and inelastic scattering included in the analysis are shown in Figs. 1 and 5–7. The curves in these figures represent the OM and CRC calculations performed with the conventional potential parameters listed in Table I. The A_i sets of these parameters were obtained with both OM and CRC fitting procedures. The B_i sets were taken from the stated references.

The OM cross sections, shown by the dashed curves ⟨OM⟩ in Figs. 1, 5, and 6, were calculated with the A_i sets of potential parameters. In these figures, the solid curves represent the coherent sum of the CRC calculations with the A_i parameters for the potential scattering, ^{7}Li reorientation (curves ⟨reor⟩) and most important transfers (see curves ⟨nn⟩, ⟨pp⟩, ⟨^{9}B⟩ for n+n-, p+p-, and ^{9}B transfers, respectively, in Fig. 1). One can see that the potential scattering dominates at forward angles (curves ⟨OM⟩) and ^{7}Li reorientation is most important at the back angles (curves ⟨reor⟩). The transfers, including α-particle transfers (curves ⟨$\alpha\alpha$⟩, ⟨α^{5}Li⟩), are negligible at all energies (see Fig. 1). All data are successfully described using the A_i parameters. Figures 5 and 6 show also the CRC-angular distributions calculated with the B_i parameters (curves ⟨B_i⟩).

One can see that the ⟨A_i⟩ and ⟨B_i⟩ curves shown in Figs. 5–7 differ significantly at large angles where the data are absent.

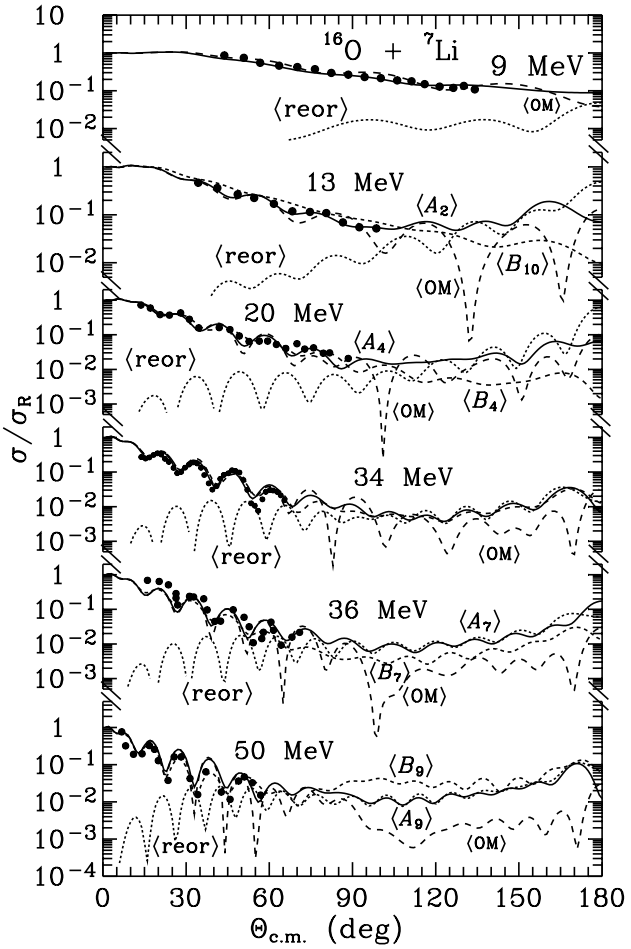

FIG. 5. Angular distributions of the ^{16}O(^{7}Li,^{7}Li)^{16}O elastic scattering at $E_{lab}(^{7}Li) = 9$ and 13 MeV [5], 20 MeV [2], 34 MeV [7], 36 MeV [4], and 50 MeV [6]. The dashed curves show the OM (curves ⟨OM⟩) and CRC angular distributions for the reorientation of ^{7}Li (curves ⟨reor⟩) calculated with the A_i parameters (see Table I). The $\langle A_i\rangle$ and $\langle B_i\rangle$ curves ($i = 2, 4, 7, 9$) represent the CRC coherent sum of potential scattering and ^{7}Li reorientation for the A_i and B_i parameters, respectively.

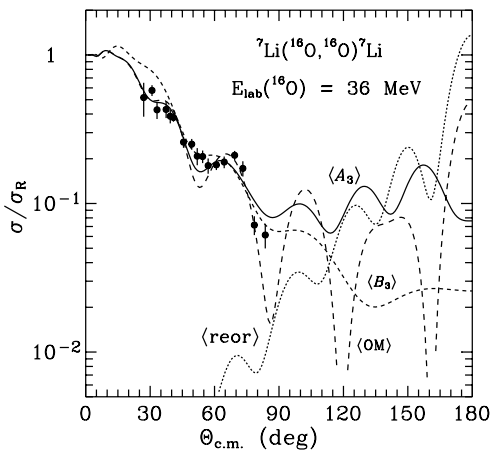

FIG. 6. Angular distribution of ^{7}Li(^{16}O,^{16}O)^{7}Li elastic scattering at $E_{lab}(^{16}O) = 36$ MeV [3]. The curves are the same as described for Fig. 5.

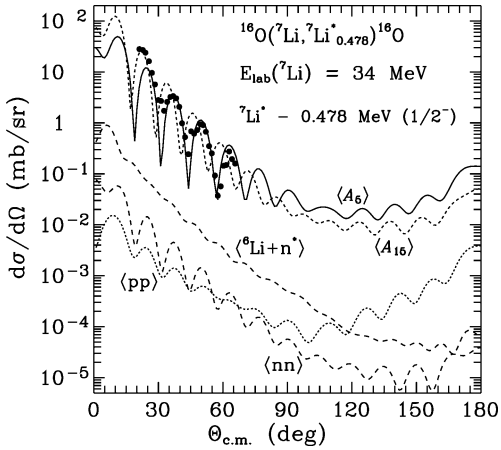

FIG. 7. Angular distribution of ^{7}Li+^{16}O inelastic scattering for the transition to the 0.478-MeV (1/2^{-}) state of ^{7}Li at $E_{lab}(^{7}Li)$= 34 MeV [7]. The curve shows the CRC-calculations for the rotational model with the A_5 and A_{15} sets of potential parameters (curves $\langle A_5\rangle$ and $\langle A_{15}\rangle$, respectively), for the neutron excitation in the ^{7}Li = ^{6}Li+n system (curve ⟨^{6}Li+n*⟩) and sequential transitions of neutrons and protons (curves ⟨nn⟩ and ⟨pp⟩, respectively).

The CRC cross sections for both sets are very close only at the energies 9 and 34 MeV (for this reason, corresponding curves are not marked). These similarities can be explained by a domination of the Coulomb scattering at low energy ($E_{c.m.} =$ 6.26 MeV) and close values of c_V and c_W (see Sec. III E and Table I) for the A_i and B_i parameters at 34 MeV.

C. Analyzing powers

Figure 2 shows the analyzing powers of $^{T}T_{10}$ and $^{T}T_{20}$ for the ^{7}Li+^{16}O elastic scattering at 42 MeV. The curves represent the CRC calculations for the ^{7}Li reorientation (dashed curves ⟨reor⟩) and coherent sum of both potential scattering and ^{7}Li reorientation (solid curves). The sum of these two processes gives a very good reproduction of the data. As Fig. 2 shows, ^{7}Li reorientation plays a very important role in producing the analyzing powers, and including the analyzing powers in the analysis makes certain that the role of ^{7}Li's reorientation is not overemphasized in the analysis.

D. Inelastic scattering

The cross sections for the excited states of ^{7}Li for ^{7}Li+^{16}O were calculated within the rotational model using the form factors

$$V_\lambda(r) = -\frac{\delta_\lambda}{\sqrt{4\pi}}\frac{dU(r)}{dr}, \qquad (1)$$

where δ_λ is the length of the λ-multipole deformation. The deformation parameters deduced in the analysis of the ^{7}Li+^{11}B scattering data [9] were used in the present calculations.

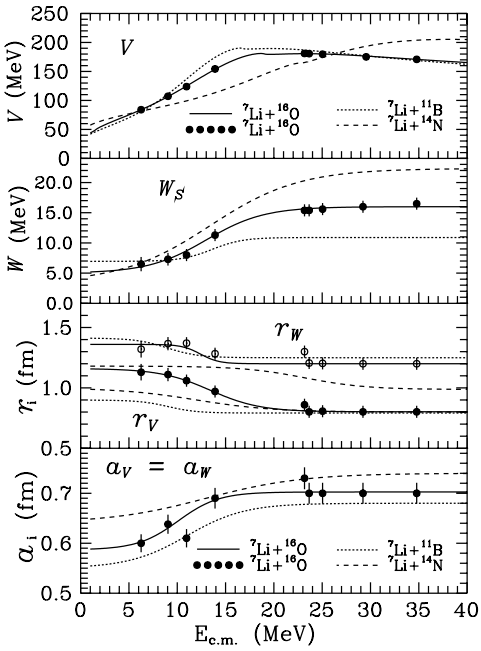

FIG. 8. Energy dependence of OM parameters for the ^{7}Li+^{16}O scattering versus the same for the scattering of ^{7}Li+^{11}B [9] and ^{7}Li+^{14}N [10].

The energy-dependent potential parameters obtained from the analysis of the elastic scattering at different energies were also used in the calculations.

At present, there is only one set of inelastic-scattering data for the system ^{7}Li+^{16}O and it consists of cross sections for the ^{7}Li 0.478-MeV state for a bombarding energy of 34 MeV ($E_{c.m.}$ = 23.65 MeV) [7]. The angular distribution of this inelastic scattering is shown in Fig. 7. The curves represent the CRC calculations for the transitions predicted by the rotational model using a ^{7}Li deformation length of $\delta_2 = 2.0$ fm [9] and A_5 and A_{15} potential parameters (curves $\langle A_5\rangle$ and $\langle A_{15}\rangle$, respectively), the single-particle excitation model for neutron excitation in the system ^{7}Li = ^{6}Li+n (curve $\langle^6$Li+n$^*\rangle$) and sequential transfers of neutrons (curve $\langle$nn$\rangle$) and protons (curve $\langle$pp$\rangle$). The A_{15} parameters were used in the CRC calculations only for the rotational model. In Fig. 7, one can see that the rotational transition dominates the cross section. The A_5

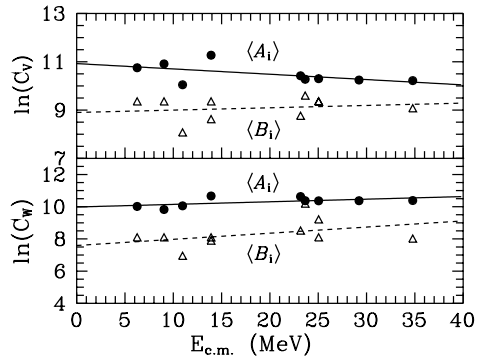

FIG. 9. Energy dependence of the c_V and c_W relations for the A_i and B_i parameters of the ^{7}Li+^{16}O scattering potential.

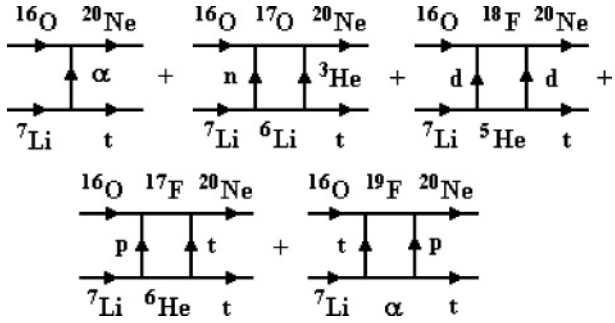

FIG. 10. Diagrams of one- and two-step transfers contributing to the ^{16}O(^{7}Li,t)^{20}Ne reaction calculations.

parameters describe the data satisfactorily except for the first oscillation maximum. They differ from the A_6 parameters for the ground state of ^{7}Li because they require larger values for the geometrical parameters r_V, r_W, a_V, and a_W. The A_{15} parameters with $a_V = a_W = 1.0$ fm describe well the first oscillation but fail in explaining others. Perhaps more data for this transition at different energies will reveal the reason behind the observed failure.

E. Energy dependence of the potential parameters

The energy dependence (ED) of the conventional potential parameters reported in Table I was fitted [9,11] with the parameters $X_i(E) = X_i^{\max}$, $X_i^{\min}$, E_{X_i}, ΔE_{X_i} (see Eqs. (10)–(13) in Ref. [9]). These parameter sets are shown in Table III and the resulting fits are shown in Fig. 8. In the analysis of the energy dependence, the dispersion relation between the real and imaginary potentials [20] was used.

The relations

$$C_V = Ve^{R_V/a_V}, \quad C_W = We^{R_W/a_W} \tag{2}$$

have been found to be useful for finding the energy dependence of the scattering potential parameters. Figure 9 shows the energy dependence of the $c_V = \ln C_V$ and $c_W = \ln C_W$ values for both A_i and B_i parameters fitted by the lines:

$$c_V(E) = \begin{cases} -0.022 \cdot E + 10.92 & \text{for } A_i \text{ sets,} \\ 0.010 \cdot E + 8.90 & \text{for } B_i \text{ sets,} \end{cases} \tag{3}$$

$$c_W(E) = \begin{cases} 0.016 \cdot E + 9.98 & \text{for } A_i \text{ sets,} \\ 0.038 \cdot E + 7.59 & \text{for } B_i \text{ sets,} \end{cases} \tag{4}$$

where $E = E_{c.m.}$. The values c_V and c_W are shown in Table I and were used to compare the parameter sets.

TABLE III. Energy dependence of the ^{7}Li+^{16}O potential parameters.

Y_i	V_0 (MeV)	W_S (MeV)	r_V (fm)	r_W (fm)	a_V (fm)	a_W (fm)
$X_i^{\min}$	92.6	5.0	0.802	1.200	0.587	0.587
$X_i^{\max}$	262.7	16.0	1.160	1.360	0.703	0.703
E_{X_i} (MeV)	13.0	13.0	13.400	12.400	10.100	10.100
ΔE_{X_i} (MeV)	3.9	3.0	2.600	0.958	2.100	2.100

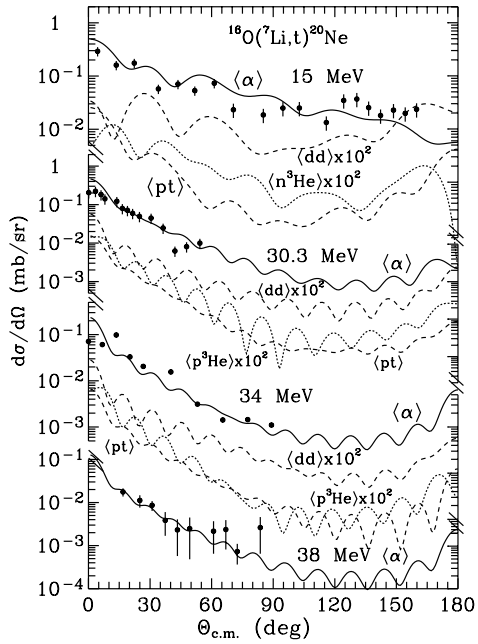

FIG. 11. Angular distributions of the ^{16}O(^{7}Li,t)^{20}Ne reaction at the energies 15 MeV [21], 30.3 MeV [22], 34 MeV [23], and 38 MeV [24]. The curves are the CRC calculations for the transfers of α cluster (curves $\langle\alpha\rangle$), $d+d$ (curves $\langle$dd$\rangle$), $p+t$ (curves $\langle$pt$\rangle$), and $n+{}^3$He (curves $\langle$n^{3}He$\rangle$).

The deduced parameters Y_i of the ^{7}Li+^{16}O scattering are listed in Table III. They can be used to calculate the Woods-Saxon potential for this channel appearing in different nuclear processes (inelastic scattering, transfer reactions, and so on) at any energy. The solid curves in Fig. 8 show the energy dependence fits of the ^{7}Li+^{16}O potential parameters.

Figure 8 shows also the energy dependence of the potential parameters for the scattering of ^{7}Li+^{11}B [9] and ^{7}Li+^{14}N [10]. One can see a remarkable difference between the parameters of these interactions, especially for the values of W_S. At the present, the origin of this difference is ambiguous. However, it may be evidence of the dependence of the nuclear interaction on either the nuclear structure of the target or a discrete ambiguity of W_S because $c_W(^{11}\mathrm{B}) \approx 7.6$, $c_W(^{14}\mathrm{N}) \approx 8.8$, $c_W(^{16}\mathrm{O}) \approx 10.3$, and $c_V(^{11}\mathrm{B}) \approx c_V(^{14}\mathrm{N}) \approx c_V(^{16}\mathrm{O}) \approx 10.4$. The difference may be resolved when more scattering data is available for CRC analysis.

F. ^{16}O(^{7}Li,t)^{20}Ne reaction

The ^{16}O(^{7}Li,t)^{20}Ne reaction data at the energies 15 MeV (12.7 MeV c.m.) [21], 30.3 MeV (23.34 MeV c.m.) [22], 34 MeV (25.95 MeV c.m.) [23], and 38 MeV (28.7 MeV c.m.) [24] were analyzed in the CRC approach to test the usefulness of the energy-dependent potential obtained in the present work for the ^{7}Li+^{16}O interaction. The diagrams of one- and two-step transfers, included in the CRC calculations, are shown in Fig. 10. The necessary spectroscopic amplitudes assumed for the calculations were found with TISM calculations and are listed in Table II. The data and CRC calculations with potential parameters C_i and D_i ($i = 1$–4) for entrance and exit channels, respectively (see Table I), are presented in Fig. 11. The parameters C_i for the ^{7}Li+^{16}O potential were calculated with ED forms [9] using ED parameters obtained in the present work (see Table III). The ^{20}Ne+t potential parameters were fitted to the reaction data. Initial conditions for the OM parameters of the exit channel were obtained from the ^{20}Ne+t elastic scattering at 2 MeV [25].

In Fig. 11, one can see that α transfer (curves $\langle\alpha\rangle$) dominates in this reaction at all energies. The sequential transfers d+d (curves $\langle$dd$\rangle$), n+^{3}He cluster (curves $\langle$n^{3}He$\rangle$) and p+t (curves $\langle$pt$\rangle$) give negligible contributions to the calculated cross sections. Thus, the obtained energy dependence of the ^{7}Li+^{16}O potential parameters can be used successfully to study the reactions induced by the ^{7}Li+^{16}O interaction.

IV. SUMMARY AND CONCLUSIONS

The angular distribution and analyzing powers $^{T}T_{10}$ and $^{T}T_{20}$ for ^{7}Li+^{16}O elastic scattering were measured at $E_{\mathrm{lab}}(^7\mathrm{Li}) = 42$ MeV. The data were explained satisfactorily within the CRC method when the reorientation of the ground state of ^{7}Li were included. This channel is especially important for reproducing the observed analyzing powers.

Existing ^{7}Li+^{16}O scattering data at the energies of $E_{\mathrm{c.m.}} = 6.26$–34.78 were then analyzed to extract energy-dependent parameters that could be used in future works. The CRC analysis of the 0.478-MeV first excited state of ^{7}Li showed that the potentials needed to describe it are different from those for the elastic channel. The deduced energy-dependent potentials differ noticeably from those found previously for the systems ^{7}Li+^{11}B and ^{7}Li+^{14}N showing that the microscopic target structure influences the scattering. An unexpected result of the analysis is that the potential parameters are relatively energy independent between 20 and 50 MeV c.m. The derived energy-dependent ^{7}Li+^{16}O potential parameters were found to yield a satisfactory description of the ^{16}O(^{7}Li,t) reaction over a wide energy range showing that they can be used in future reaction studies.

ACKNOWLEDGEMENT

The Florida State group acknowledges support of the U. S. National Science Foundation.

[1] H. Nishioka, J. A. Tostevin, R. C. Johnson, and K.-I. Kubo, Nucl. Phys. **A415**, 230 (1984).
[2] K. Bethge, C. M. Fou, and R. W. Zurmühle, Nucl. Phys. **A123**, 521 (1969).
[3] J. Orloff and W. W. Daehnick, Phys. Rev. C **3**, 430 (1971).
[4] P. Schumacher *et al.*, Nucl. Phys. **A212**, 573 (1973).
[5] J. E. Poling, E. Norbeck, and R. R. Carlson, Phys. Rev. C **13**, 648 (1976).

[6] J. Cook, K. W. Kemper, P. V. Drumm, L. K. Fifield, M. A. C. Hotchkis, T. R. Ophel, and C. L. Woods, Phys. Rev. C **30**, 1538 (1984).
[7] K. W. Kemper, G. A. Hall, S. P. Van Verst, and J. Cook, Phys. Rev. C **38**, 2664 (1988).
[8] I. J. Thompson, Comput. Phys. Rep. **7**, 167 (1988).
[9] A. A. Rudchik *et al*., Phys. Rev. C **72**, 034608 (2005).
[10] A. T. Rudchik *et al*., Nucl. Phys. **A700**, 25 (2002).
[11] A. T. Rudchik *et al*., Nucl. Phys. **A677**, 61 (2000).
[12] A. J. Mendez *et al*., Nucl. Instrum. Methods A **329**, 37 (1993).
[13] P. D. Cathers *et al*., Nucl. Instrum. Methods A **457**, 509 (2001).
[14] P. D. Cathers *et al*., Phys. Rev. C **63**, 064601 (2001).
[15] B. S. Nilsson, SPI-GENOA: An Optical Model Search Code, Niels Bohr Institute Report, 1976.
[16] Yu. F. Smirnov and Yu. M. Tchuvil'sky, Phys. Rev. C **15**, 84 (1977).
[17] A. T. Rudchik and Yu. M. Tchuvil'sky, a code DESNA, The Kiev Institute for Nuclear Research report KIYAI-82-12 (1982).
[18] A. T. Rudchik and Yu. M. Tchuvil'sky, Ukr. Fiz. Zh. **30**, 819 (1985).
[19] A. N. Boyarkina, Structure of 1_p shell nuclei, Moscow State University Report (1973).
[20] C. Mahaux, H. Ngo, and G. R. Satchler, Nucl. Phys. **A449**, 354 (1986).
[21] R. Middleton, In *Proceedings of the International Conference on Nuclear Reactions Induced by Heavy Ions*, edited by R. Bock and W. R. Hering (North-Holland, Amsterdam, 1970), p. 263.
[22] V. Z. Goldberg *et al*., Izv. Akad. Nauk SSSR, Ser. Fiz. **33**, 579 (1969); Bull. Acad. Sci. USSR, Phys. Ser. **33**, 536 (1970).
[23] S. G. Cooper, J. Phys. G: Nucl. Phys. **12**, 371 (1986).
[24] M. E. Cobern, D. J. Pisano, and P. D. Parker, Phys. Rev. C **14**, 491 (1976).
[25] G. H. Herling, L. Cohen, and J. D. Silverstein, Phys. Rev. **178**, 1551 (1969).